# Hydrometeor Shape Variability in Snowfall as Retrieved from Polarimetric Radar Measurements

SERGEY Y. MATROSOV

Cooperative Institute for Research in Environmental Sciences, University of Colorado Boulder, and NOAA Physical Sciences Laboratory, Boulder, Colorado

#### ALEXANDER V. RYZHKOV

Cooperative Institute for Mesoscale Meteorological Studies, University of Oklahoma, and NOAA Severe Storms Laboratory, Norman, Oklahoma

#### Maximilian Maahn<sup>a</sup> and Gijs de Boer

Cooperative Institute for Research in Environmental Sciences, University of Colorado Boulder, and NOAA Physical Sciences Laboratory, Boulder, Colorado

(Manuscript received 11 March 2020, in final form 28 July 2020)

ABSTRACT: A polarimetric radar–based method for retrieving atmospheric ice particle shapes is applied to snowfall measurements by a scanning  $K_a$ -band radar deployed at Oliktok Point, Alaska (70.495°N, 149.883°W). The mean aspect ratio, which is defined by the hydrometeor minor-to-major dimension ratio for a spheroidal particle model, is retrieved as a particle shape parameter. The radar variables used for aspect ratio profile retrievals include reflectivity, differential reflectivity, and the copolar correlation coefficient. The retrievals indicate that hydrometeors with mean aspect ratios below 0.2–0.3 are usually present in regions with air temperatures warmer than approximately from  $-17^{\circ}$  to  $-15^{\circ}$ C, corresponding to a regime that has been shown to be favorable for growth of pristine ice crystals of planar habits. Radar reflectivities corresponding to the lowest mean aspect ratios are generally between -10 and 10 dBZ. For colder temperatures, mean aspect ratios are typically in a range between 0.3 and 0.8. There is a tendency for hydrometeor aspect ratios to increase as particles transition from altitudes in the temperature range from  $-17^{\circ}$  to  $-15^{\circ}$ C toward the ground. This increase is believed to result from aggregation and riming processes that cause particles to become more spherical and is associated with areas demonstrating differential reflectivity decreases with increasing reflectivity. Aspect ratio retrievals at the lowest altitudes are consistent with in situ measurements obtained using a surface-based multiangle snowflake camera. Pronounced gradients in particle aspect ratio profiles are observed at altitudes at which there is a change in the dominant hydrometeor species, as inferred by spectral measurements from a vertically pointing Doppler radar.

KEYWORDS: Cloud retrieval; Radars/Radar observations

### 1. Introduction

The shapes of ice hydrometeors in the atmosphere can vary significantly. Accounting for these shapes (at least in a mean sense) is important for many practical applications. One such application is quantitative precipitation estimation (QPE) in snowfall. Most modern weather radars have polarimetric capabilities, which allow for enhancing snowfall QPE methods compared to traditional reflectivity-based techniques. The efficient use of polarimetric measurements in new weather radarbased snowfall QPE methods, however, requires knowledge or appropriate assumptions about mean hydrometeor shapes and their variability (e.g., Bukovčić et al. 2018).

Hydrometeor shape (habit) information is also essential for in depth microphysical studies of cloud and precipitation processes. Advanced microphysical models (e.g., Hashino and Tripoli 2008; Jensen et al. 2017) consider nonspherical

Corresponding author: Sergey Y. Matrosov, sergey.matrosov@noaa.gov

hydrometeor shapes, which influence particle growth by vapor deposition, riming, and aggregation processes. Observation-based estimates of hydrometeor shapes and their variability can lead to better microphysical parameterizations of these processes and thus enhancement of weather and climate models by incorporating more realistic representation of cloud and precipitation processes.

Ice hydrometeors have a multitude of different habits and are often irregular in shape. Traditionally, only a few predefined ice hydrometeor categories are considered in radar-based hydrometeor identification schemes and numerical model parameterizations. Such categories usually include single ice crystals, aggregates, hail, and graupel. It is typically assumed that particles in each hydrometeor category have a certain aspect ratio (defined as a shape parameter representing the ratio of particle minor-tomajor dimensions). Aspect ratios of ice hydrometeors, however, vary rather widely and change as particles evolve even if they still remain within a given category. An aspect ratio parameter is also used to characterize a general shape of irregular shape particles (e.g., Korolev and Isaac 2003; Garrett et al. 2015).

<sup>&</sup>lt;sup>a</sup> Current affiliation: Leipzig University, Leipzig, Germany.



FIG. 1. The AMF3 radars deployed at Oliktok Point.

Polarimetric radar measurements have been used to retrieve ice hydrometeor aspect ratios assuming spheroidal (Matrosov et al. 2001; Myagkov et al. 2016) or solid ice hexagonal prism particles (Melnikov 2017) and a Rayleigh type of scattering, which is valid when particles are much smaller than the radar wavelength. Particle densities, however, are usually smaller than those of solid ice, so meaningful retrievals also require an assumption of density, which, in addition to particle shape, strongly influences observed radar variables (e.g., Heymsfield et al. 2005). A recent generalization of the polarimetric radar approach (Matrosov 2020) for aspect ratio retrievals accounts for changing particle density. The spheroidal shape, which is often used in modeling (e.g., Jensen et al. 2017) and QPE (Ryzhkov and Zrnić 2019) studies, is assumed for these retrievals as it was shown to adequately describe observed polarimetric radar variables in many practical cases (e.g., Reinking et al. 2002; Matrosov et al. 2012).

The main objective of this study was to evaluate the variability of ice hydrometeor aspect ratios in Arctic snowfall based on polarimetric radar-based retrievals. Information on shape variability can be useful for understanding where in the cloud layer nucleation takes place and to what extent other microphysical processes (e.g., depositional growth, riming, and aggregation) contribute to the evolution of the ice crystal population during fallout. Of particular interest was exploring the variability of aspect ratios with temperature, which varies with height above the ground. Of specific interest to this study were also the mean correspondences between conventional radar variables (e.g., radar reflectivity) and polarimetric measurables such as differential reflectivity, with the latter being sensitive to hydrometeor shape and the most common directly observable polarimetric radar variable. Another objective of this study was to assess the potential of the radar-based shape retrievals to observe the microphysical processes dominating particle habit evolution in solid precipitation (e.g., riming and/or aggregation).

#### 2. Snowfall event of 21 October 2016

The observational data for this study were collected at the U.S. Department of Energy (DOE) Atmospheric Radiation Measurement (ARM) Program Mobile Facility 3 (AMF3) deployed at Oliktok Point, Alaska (70.495°N, 149.886°W). This facility is equipped with a vertically pointing Ka-band (34.83 GHz) ARM zenith-pointing radar (KAZR), which measures Doppler spectra (Kollias et al. 2020). In addition to the KAZR, a second-generation scanning ARM cloud radar (SACR2) was operational at this site during 2016-17. The SACR2 system is a fully polarimetric dual-frequency (35.29 and 93.93 GHz) radar with alternate transmission of horizontally and vertically (h-v) polarized pulses (Kollias et al. 2020). The polarimetric variables directly measured by the SACR2 include differential reflectivity  $Z_{DR}$ , differential phase shift, linear depolarization ratio (LDR), and the copolar correlation coefficient  $\rho_{hv}$ . Figure 1 shows the radars at the AMF3 site.

Figures 2a and 2b show time-height cross sections of KAZR radar reflectivity factor (hereinafter reflectivity  $Z_e$ ), and measurements of mean vertical Doppler velocity  $V_D$  (Matthews et al. 2015) during a significant snowfall event observed on 21 October 2016. This event was of particular interest because it comprised a large variety of snowfall conditions. Additionally, in situ ice particle sampling was available, which indicated the existence of a great variety of particle types ranging from single pristine crystals to heavily aggregated and rimed snowflakes. Reflectivities during this event varied across a wide range, sometimes reaching around 23 dBZ, which is among the highest  $K_a$ -band  $Z_e$ 

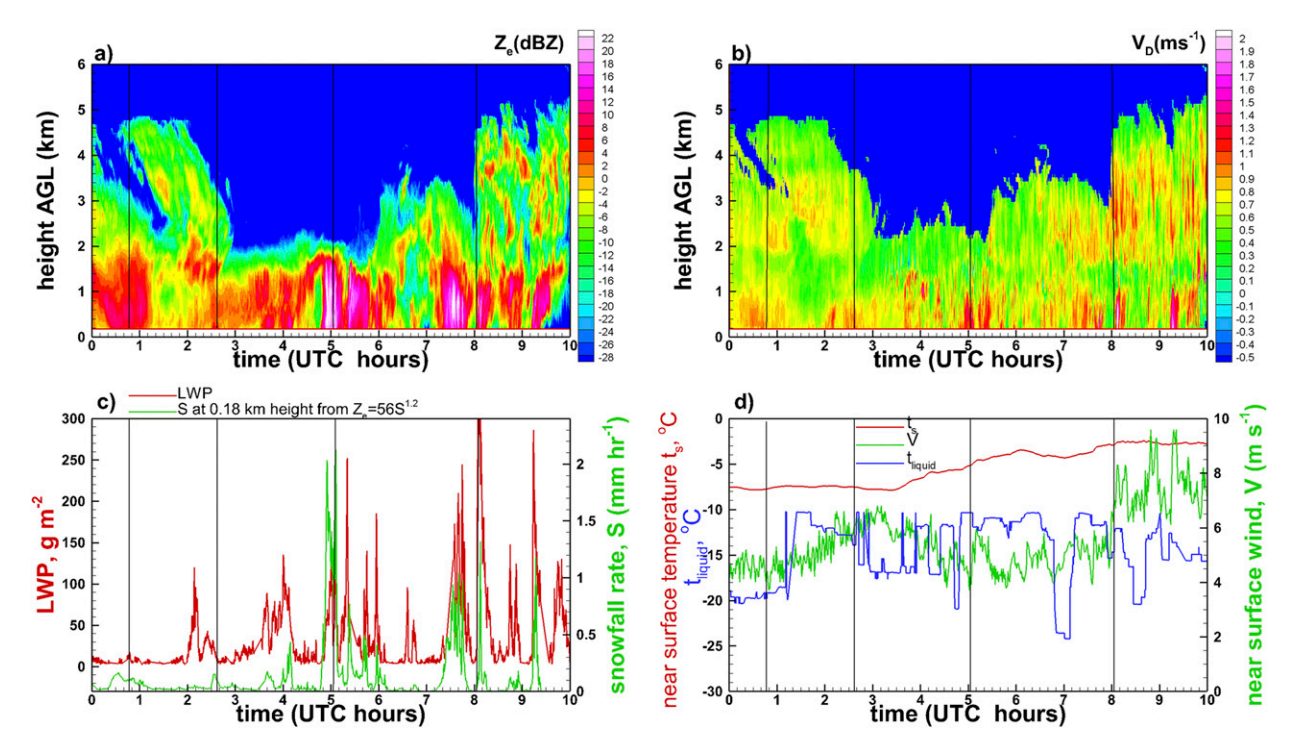


FIG. 2. Time-height cross sections of AMF3 KAZR (a) reflectivity and (b) mean vertical Doppler velocity (positive velocities are downward) measurements for the event observed on 21 Oct 2016. (c) Time series of LWP (red) and snowfall rate (green). (d) Standard near surface air temperature (red) and horizontal wind speed (green) measurements and retrieved mean temperature of supercooled liquid (blue). Thin vertical lines in (a)–(d) show the midpoint of the time intervals for which aspect ratio retrievals in Figs. 3 and 4 (below) are shown.

values observed in the AMF3 snowfalls (e.g., Matrosov et al. 2019). Such high reflectivity values suggest populations of larger hydrometeors as there is a significant correlation between  $Z_e$  and characteristic particle size (e.g., Matrosov 1997). For some time periods (e.g., around 0500, 0810, and 0920 UTC), downward mean Doppler velocities in lower atmospheric layers were in excess of about  $1.5 \,\mathrm{m\,s^{-1}}$ , which is indicative of significant riming of the observed hydrometeors (Mosimann 1995; Vogel and Fabry 2018).

Figure 2c depicts supercooled liquid water path (LWP) and estimates of instantaneous snowfall rate S during the 21 October 2016 event. These estimates were calculated using KAZR reflectivities and a  $K_a$ -band relation  $Z_e(mm^6m^{-3}) = 56S(mmh^{-1})^{1.2}$ . This relation was found to satisfactorily approximate total liquid equivalent snow accumulations (Matrosov et al. 2008). Because of the KAZR "blind zone," snowfall rates in Fig. 2c correspond to a height of 0.17 km above the ground.

LWP values and mean liquid temperature  $t_{\rm liquid}$  shown in Fig. 2d were retrieved from measurements of the three-channel microwave radiometer operating at frequencies of 90, 31.4, and 23.8 GHz. The LWP retrieval "dry bias" was accounted for. Periods of elevated LWP values were interleaved by periods of absence of supercooled liquid in a vertical atmospheric column. Mean liquid temperature was retrieved using a technique described by Matrosov and Turner (2018). As seen from Fig. 2d, the corresponding  $t_{\rm liquid}$  values were for the most part between  $-20^{\circ}$  and  $-10^{\circ}$ C. The air temperature through the whole atmospheric vertical column was below freezing and the

near surface air temperature during this event was approximately between  $-7^{\circ}$  and  $-3^{\circ}$ C.

As seen from Fig. 2c, periods of higher LWP and reflectivity often coincide with increased reflectivities and snowfall rates (e.g., around 0500, 0730, 0810, and 0920 UTC). This might be explained by increased snowflake masses via collection of available supercooled liquid as a result of riming, which leads to an intensification of vertical snow flux. One exception to this correlation is the time period around 0030 UTC, where an increased snowfall rate is observed without any notable rise in LWP. Depositional snowflake growth might contribute to such an increase. Periods of elevated supercooled LWP, however, do not always correspond to the times of snowfall rate increases (e.g., around 0210, 0635, and 0945 UTC).

Overall, observed environmental conditions, hydrometeor types, and radar measurables varied rather widely during the snowfall event of 21 October 2016. In situ hydrometeor images from the multiangle snowflake camera (MASC) (Garrett et al. 2015) deployed at the radar site were also available throughout this event. These factors make it instructive to analyze the radar-based retrievals of hydrometeor shapes for this event in detail.

#### a. Retrieval approach

Although differential reflectivity  $Z_{\rm DR}$  is sensitive to the shape of hydrometeors, it is also rather strongly affected by their orientation. The h-v polarization-based LDR variable is

also very strongly affected by particle orientation. This variable is also very noisy because the cross-polarized radar echoes are usually very weak (e.g., by 1–3 orders of magnitude weaker than the copolarized echoes). Therefore, reliable LDR measurements exist in much more limited atmospheric regions relative to other variables (e.g., reflectivity) and are only reliably available where signal-to-noise ratio (SNR) of cross-polarized echoes is sufficiently high (e.g., > 5 dB).

While directly measured SACR2 polarimetric variables are not very suitable for practical hydrometeor shape retrievals, they can be used to reconstruct a depolarization ratio (DR), which is a proxy for circular depolarization ratio  $C_{\rm dr}$  and can be expressed as (Melnikov 2017; Ryzhkov et al. 2017; Matrosov et al. 2017)

$$C_{\rm dr} = (Z_{\rm dr} + 1 - 2Z_{\rm dr}^{0.5} \rho_{hv})(Z_{\rm dr} + 1 + 2Z_{\rm dr}^{0.5} \rho_{hv})^{-1}.$$
 (1)

The  $Z_{\rm dr}$  in (1) is in linear units [as opposed to the  $Z_{\rm DR}$  notations typically used when these variables are expressed in the logarithmic units (i.e., decibels)]. LDR data were neglected in  $C_{\rm dr}$  estimates (Matrosov et al. 2017). Relative to  $Z_{\rm DR}$  and LDR, CDR $_p$  [CDR $_p$  =10 log $_{10}(C_{\rm dr})$ ] is much less susceptible to particle orientations, especially at radar beam elevation angles of approximately 40° (Matrosov et al. 2017), and, since the crosspolar measurements are not involved in estimating CDR $_p$ , it is usually available in the same atmospheric volumes in which copolar radar variables reliably exist.

The CDR<sub>p</sub>-based aspect ratio retrieval technique, as applied to the K<sub>a</sub>-band SACR2 measurements during range-height indicator (RHI) radar scans, is described in detail by Matrosov et al. (2017). Since  $CDR_p$ -based aspect ratio relations depend on characteristic particle size, this technique was enhanced by the use of reflectivity-based estimates of hydrometeor median volume size  $D_{mv}$ . Including these estimates allows for indirect accounting of non-Rayleigh scattering and changing hydrometeor bulk density with increasing particle characteristic size Matrosov (2020). A mean  $K_a$ -band  $D_{mv}$ - $Z_e$  relation for an exponential particle size distribution (Matrosov and Heymsfield 2017) was further used. The retrievals were performed assuming oblate particle shapes. Such shapes were assumed because elevation angle dependencies of CDR<sub>p</sub> (i.e., minimal depolarization values observed near the zenith viewing direction and a general increase in CDR<sub>p</sub> with a transition toward a slant-viewing beam orientation) indicated the dominance of planar ice hydrometeor habits of precipitating hydrometeors (e.g., Matrosov et al. 2017).

During the Oliktok Point deployment, the SACR2 operated in 30-min cycles. Each cycle included four hemispheric (0°–180° radar elevations with an increment of 0.3°) RHI scans with the elevation angle changes in the azimuthal directions of 0°, 45°, 90°, and 135° (Hardin et al. 2011); three plan position indicator (PPI) scans at radar elevation angles of 3°, 5°, and 20° (Isom et al. 2018); and several minutes of measurements with a vertically pointing radar beam. The SACR2 radar range gate spacing is 0.03 km. The RHI scan sequence took approximately 6 min to complete.

#### b. Particle shape retrieval results

Figure 3 shows retrievals of vertical profiles of hydrometeor average aspect ratios for several periods during the

event of 21 October 2016. The retrievals were performed on measurements from SACR2 RHI scans with beam pointing azimuths at  $40^{\circ} \pm 3^{\circ}$  elevation angles  $\alpha$  and were averaged and recalculated to heights above ground level (AGL) as  $h = R \sin(\alpha)$ , where R is the radar range. Such geometry choice was dictated by the lowest sensitivity of CDR<sub>p</sub> to particle orientations at elevation angles of around  $40^{\circ}$  (Matrosov et al. 2017). Additional five range gate averaging of retrieval results along the slant beam was performed to reduce retrieval noise. The height increment in the Fig. 3 retrievals is  $0.1 \, \mathrm{km}$ .

Aspect ratio retrieval uncertainties from SACR2 measurements are estimated to be around 0.15 as indicated by the theoretical assessment and comparisons with in situ observations (Matrosov et al. 2017). On average, two 6-min time intervals of retrievals were available per 1 h of radar measurements. Retrievals were additionally thresholded at  $\rho_{hv} > 0.8$  to reduce the influence of ground clutter.

Although the uncertainties associated with this retrieval are significant, trends and variability of particle mean aspect ratios in Fig. 3 are identifiable. Modest particle aspect ratio changes as a function of the radar beam azimuth angle at a given height (e.g., Figs. 3a,b) indicate that particle shapes in a "retrieval cone" defined by the 40° radar beam elevation do not significantly vary during the 6-min-long SACR2 RHI scanning intervals. Larger aspect ratio changes from one azimuthal direction to another (i.e., in Fig. 3c except near the ground, and in Fig. 3d) are likely due to increased spatial and/or temporal variability of hydrometeor mean shapes within this cone.

Figure 4 depicts SACR2 reflectivity measurements at different azimuthal directions corresponding to the aspect ratio retrievals in Fig. 3. As with particle aspect ratios, the observed variability of reflectivity within the "retrieval cone" was larger for some RHI scan intervals than for others. The strongest reflectivity variability was observed during the RHI scans just after 0800 UTC (Fig. 4d).

For many hydrometeor aspect ratio profiles (Fig. 3), a distinct change in particle shape starts occurring just below approximately a 2-km altitude. To investigate the cause of this, measurements from the twice-daily (~1730 and ~2330 UTC) radiosondes launched at Oliktok Point were used, with the closest in time sounding results shown by Matrosov et al. (2017, their Fig. 6). In addition to aspect ratios and reflectivities Figs. 3 and 4 also show temperature profiles for the middle of the corresponding RHI scan intervals as interpolated from two consecutive radiosonde launches (e.g., Giangrande and Toto 2013). According to these profiles, a 2-km altitude corresponds to ambient air temperatures approximately from  $-15^{\circ}$  to  $-17^{\circ}$ C, a range favorable for the growth of planar-type ice crystals such as single dendrites and hexagonal plates (Magono and Lee 1966; Bailey and Hallett 2009). Such pristine crystals generally have aspect ratios smaller than 0.1-0.2 (e.g., Pruppacher and Klett 1978).

#### c. Hydrometeor images

Figure 5 shows images of ice hydrometeors observed by the MASC during the four SACR2 RHI measurement periods

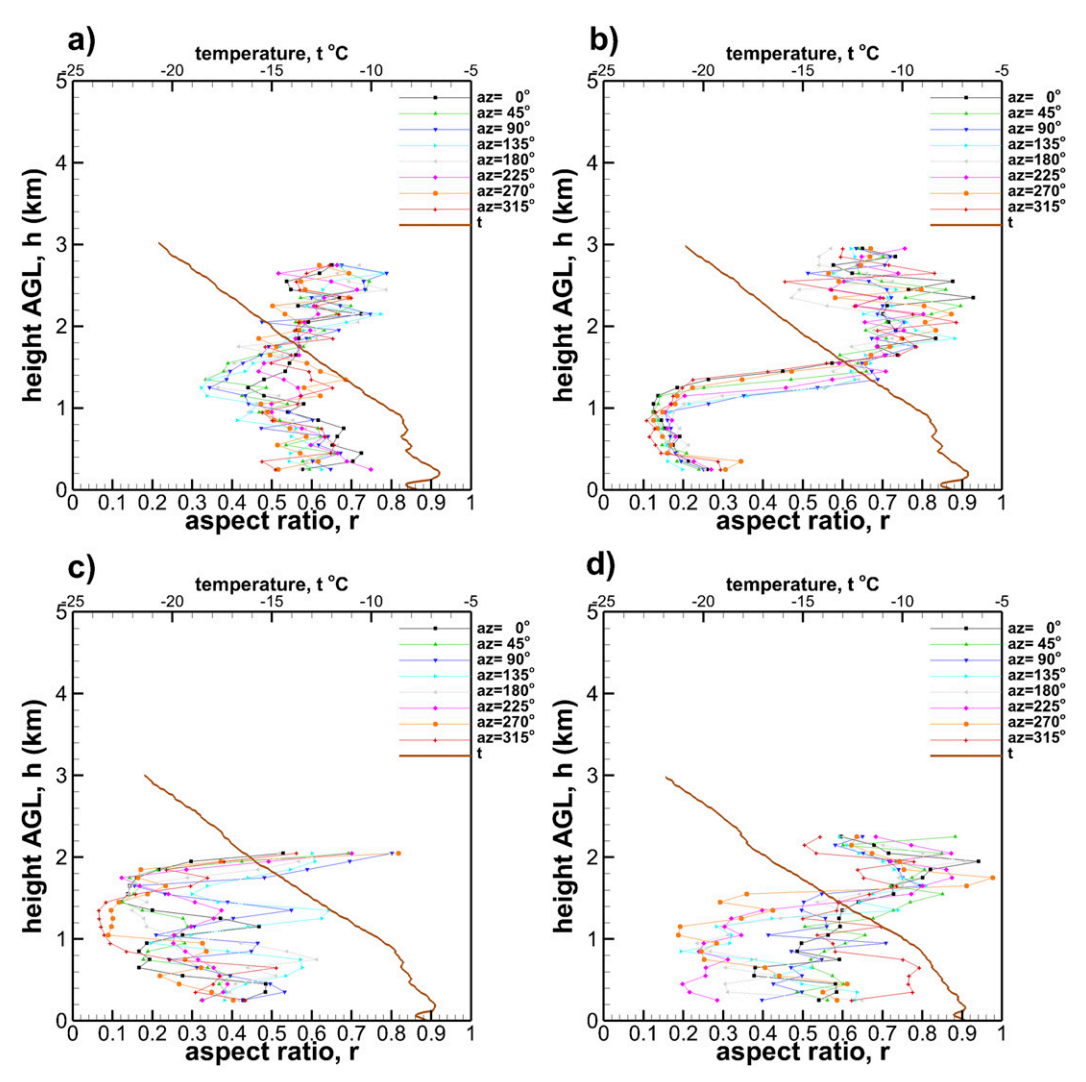


FIG. 3. Hydrometeor aspect ratio retrievals for four 6-min RHI time intervals during a snowfall observed on 21 Oct 2016. Interval start times are (a) 0044, (b) 0234, (c) 0500, and (d) 0800 UTC. Retrievals are shown for different azimuthal directions. The thick brown curve shows the temperature profile (upper x axis) for the middle of the corresponding time intervals.

shown in Figs. 3 and 4 (The rows marked "a"-"d" in Fig. 5 correspond to the respective periods shown in Figs. 3a-d and 4a-d). MASC data processing was completed by Maahn (2019). While MASC measurements cannot be used for reliable reconstruction of particle size distributions due to the small sample size, they provide good visual information on the types and habits of hydrometeors determining radar echoes at the lowest altitudes.

As seen from row a in Fig. 5, which corresponds to the SACR2 RHI scanning period between about 0044 and 0050 UTC, hydrometeors typical for this time period were mostly smaller (~1–1.5 mm) aggregates of irregular shapes. LWP values during this period were very low (Fig. 2c), particles were mostly unrimed and there was little variability in a general particle type. Observed reflectivity and hydrometeor aspect ratio retrieval profiles for this period (Figs. 3a and 4a)

did not exhibit much variability either. Aspect ratios retrieved from radar measurements near the ground were in a range of about 0.5–0.8, which is general agreement with those from the MASC images.

MASC images of hydrometeors during the 0234–0240 UTC RHI scanning period are mostly hexagonal plates (e.g., image b1 in Fig. 5) and single pristine dendrites (e.g., images b2, b3, and b4 in Fig. 5). Modest amounts of supercooled liquid were present during this time period (Fig. 2c) and some of the observed crystals were relatively lightly rimed. These crystal types have very low aspect ratios. This is consistent with the radar-based hydrometeor shape retrievals (Fig. 3b), which indicate the dominance of very low aspect ratio particles in an atmospheric layer below the height of about 1.3 km. Retrieved aspect ratios tend to increase in the lowest 0.4-km layer, which is likely due to some modest amount of aggregation. Around

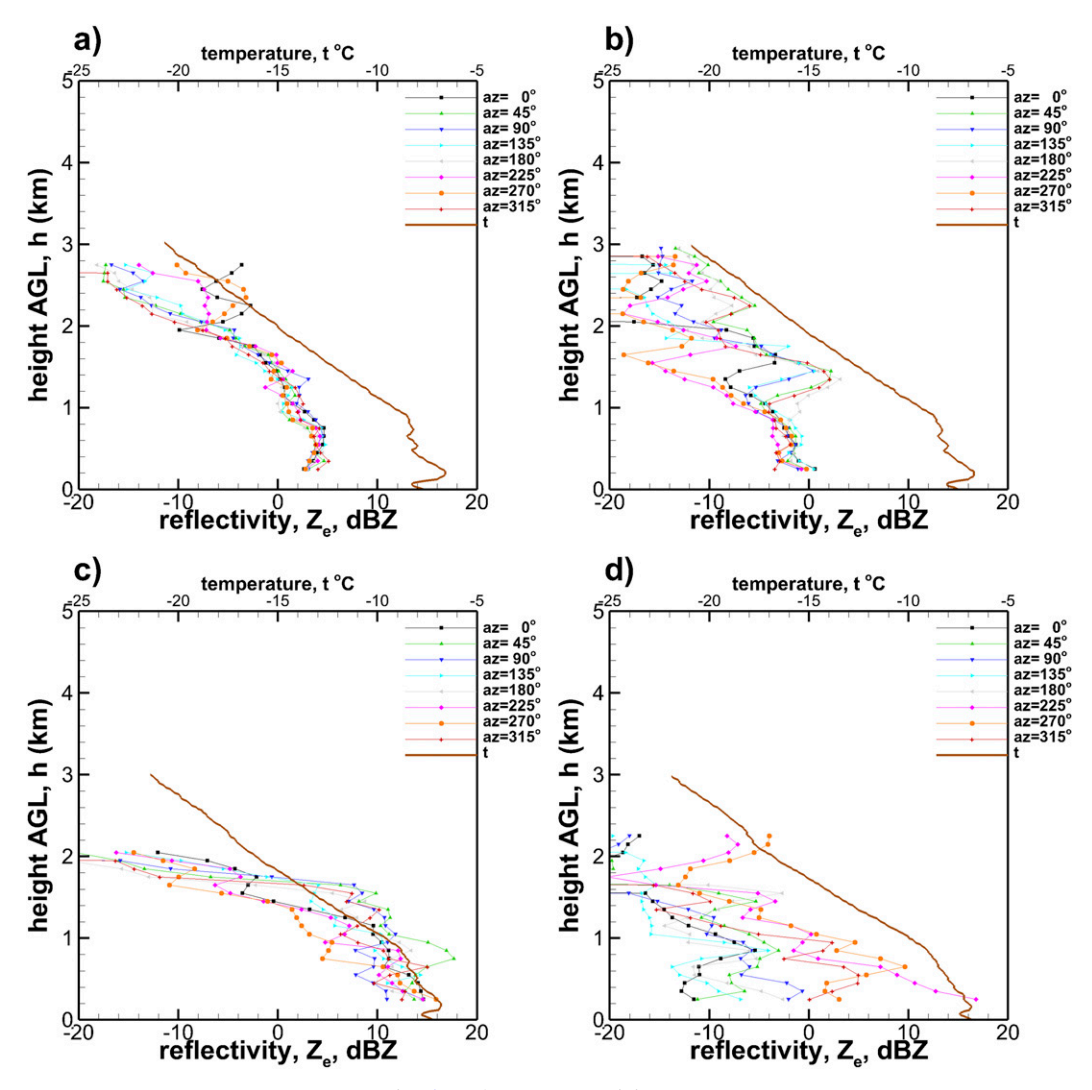


FIG. 4. As in Fig. 3, but for Reflectivity measurements.

this time, simple plate aggregates were also observed at low altitudes by a balloon borne particle sampler (Matrosov et al. 2017).

Retrieved aspect ratios in the layer below 1.3 km are in the range approximately between 0.1 and 0.3, and, given retrieval uncertainties of around 0.15 (Matrosov et al. 2017), they appropriately correspond to typical aspect ratios of crystals of the types observed at the ground (e.g., Pruppacher and Klett 1978). This correspondence suggests that the spheroidal particle shape assumption is suitable for particles with low aspect ratios, although precise retrievals of low aspect ratios are not possible because of existing retrieval uncertainties and limitations of bulk-density spheroidal shape model for such particles (e.g., Schrom and Kumjian 2018).

The SACR2 RHI scanning period in the interval approximately between 0500 and 0506 UTC was characterized by larger reflectivities and snowfall rates. Hydrometeors of different types were observed by the MASC during this interval (row c in Fig. 5), including rimed aggregates (images c1 and c2

in Fig. 5) and pristine and rimed dendrites (images c3 and c4 in Fig. 5). Retrieved aspect ratios for hydrometeors near the ground were around 0.4 (Fig. 3c), which might be an appropriate mean value for a mix of very nonspherical and quasi-spherical particles. The variability of retrieved hydrometeor aspect ratio values aloft (e.g.,  $\sim$ 1.2 km) during this time period is very high. These values are very low ( $\sim$ <0.1) along some radar beam azimuthal directions. Such low aspect ratio values are indicative of unrimed pristine crystals, as found in the particle mixture near the ground.

The highest variability of retrieved hydrometeor aspect ratios and measured reflectivities was observed during the SACR2 RHI scanning interval between 0800 and 0806 UTC (Figs. 3d and 4d). This interval was also characterized by the largest amounts of supercooled LWP (Fig. 2c). The MASC images during this interval (row d in Fig. 5) indicate hydrometeors ranging from moderately rimed dendrites to graupel-like particles. Aspect ratios of such hydrometeors

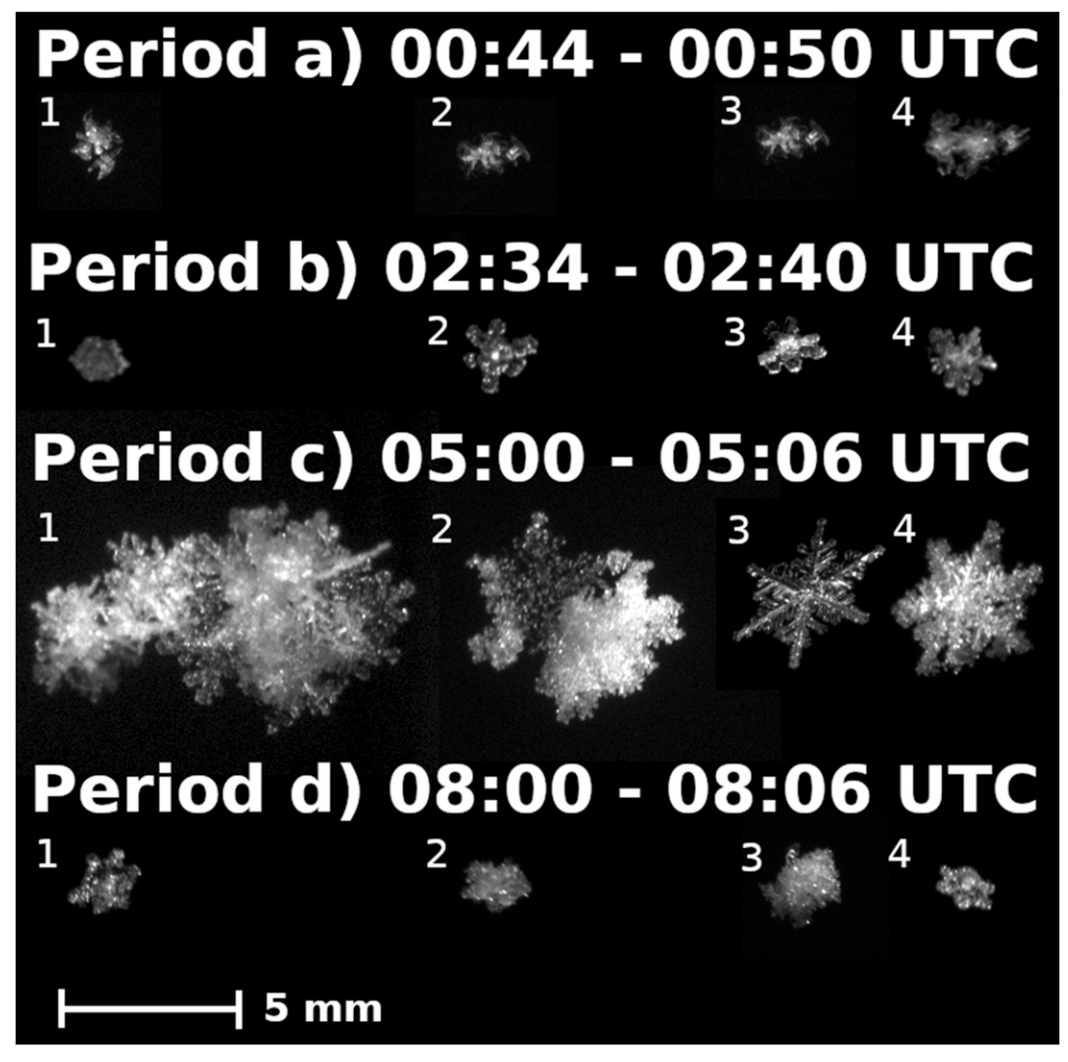


FIG. 5. MASC images of typical ice hydrometeors taken during SACR2 RHI scans intervals on 21 Oct 2016. The rows labeled "a"-"d" respectively correspond to the intervals shown in Figs. 3a-d and 4a-d.

vary significantly, which is also manifested in the corresponding retrievals.

### d. Vertical profiles of Doppler spectra

Analyzing profiles of Doppler spectra from the vertically pointing KAZR can provide additional information to help shed further light on some of the polarimetric SACR2-based retrievals of aspect ratios discussed above. Figure 6 depicts KAZR time-height cross sections of mean vertical Doppler velocities during the SACR2 RHI scan periods analyzed above (Figs. 3–5). The KAZR is more sensitive than the SACR2, so it observes some cloud echoes beyond the highest level available from the SACR2 data (Figs. 3 and 4). The lowest liquid cloudbase estimates from the collocated laser ceilometer are also shown in Fig. 6 as indicated by the black lines. Note that direct ceilometer cloud-base estimates were not available for the period shown in Fig. 6c, which is likely due to heavier snowfall

during the corresponding time interval. The cloud-base estimates shown in Fig. 6c are interpolated data from available ceilometer measurements at 0452 and 0507 UTC.

Vertical profiles of KAZR Doppler spectra for six different representative times during the snowfall event of 21 October 2016 are shown in Fig. 7. These times are marked by vertical lines in Fig. 6. Doppler spectra did not change significantly during the 0044–0050 and 0234–0240 UTC SACR2 RHI scans, so only spectra for approximate middle time moments of these intervals are shown.

The Doppler spectra corresponding to approximately 0047 UTC (Fig. 7a) are suggestive of the existence of two distinct hydrometeor species in a vertical profile, species 1 and species 2. According to the terminology used by Griffin et al. (2018) and Oue et al. (2018), species 1 and 2 represent quasi-spherical or isometric (I type) and dendritic (D type) ice particles, respectively. I-type particles include a broad category of snow

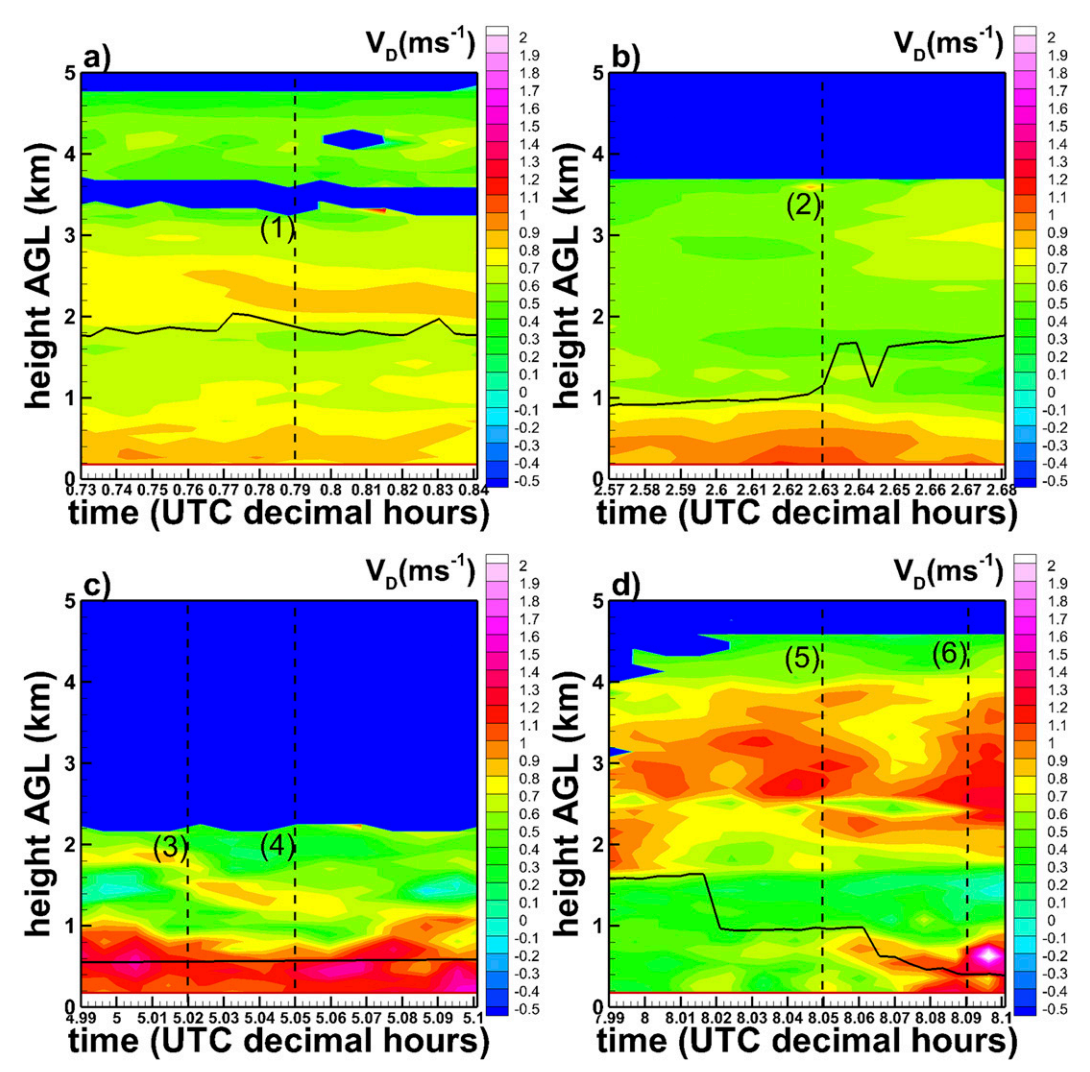


FIG. 6. KAZR vertical Doppler velocity cross sections for four SACR2 RHI scanning periods on 21 Oct 2016: (a) 0044–0050, (b) 0234–0240, (c) 0500–0506, and (d) 0800–0806. Solid black lines show lowest liquid cloud-base returns from ceilometer measurements. Vertical dashed lines show times of the Doppler spectra depicted in Fig. 7, below.

aggregates and ice crystals with irregular or moderately non-spherical shapes with average aspect ratios approximately between 0.5 and 0.7. The D-type crystals are comprised of highly oblate (dendrites or hexagonal plates) or prolate (needles) hydrometeors with very low aspect ratio (usually less than 0.2). The I-type ice particles can appear at all heights and temperatures above the melting layer (Korolev and Isaac 2003), whereas the D-type crystals grow locally in a layer centered at  $-15^{\circ}$ C (planar particles) or at  $-6^{\circ}$ C (columnar particles) (Fukuta and Takahashi 1999).

At 0047 UTC species 1 is seen throughout the entire vertical profile and it is dominant at all heights while species 2 is generated at heights of  $\sim$ 2.0–2.3 km, corresponding to air temperatures approximately from  $-17^{\circ}$  to  $-15^{\circ}$ C. This second species can be traced independently as a secondary Doppler spectrum maximum down a height of  $\sim$ 1.4 km. It then merges

with species 1 and there is no evidence of two distinct hydrometer species below this height. It is hypothesized that species-2 particles are single dendritic and/or hexagonal plate crystals, generated in the temperature range favorable for the growth of these particle types. A local minimum in mean hydrometeor aspect ratio retrievals, which is observed at heights of about 1.2–1.6 km for most SACR2 beam azimuthal directions for the 0044–0050 UTC period (Fig. 3a), is also consistent with existence of single planar crystals in a mix with more spherical particles.

As in the Doppler measurements at 0047 UTC, the Doppler spectrum at around 0238 UTC (Fig. 7b) shows the existence of the two main hydrometeor species in a vertical profile. In this case, however, species 2 (i.e., dendrites and/or hexagonal plates) can be traced distinctively from the heights of their generation to the ground level. Species-1 ice hydrometeors are

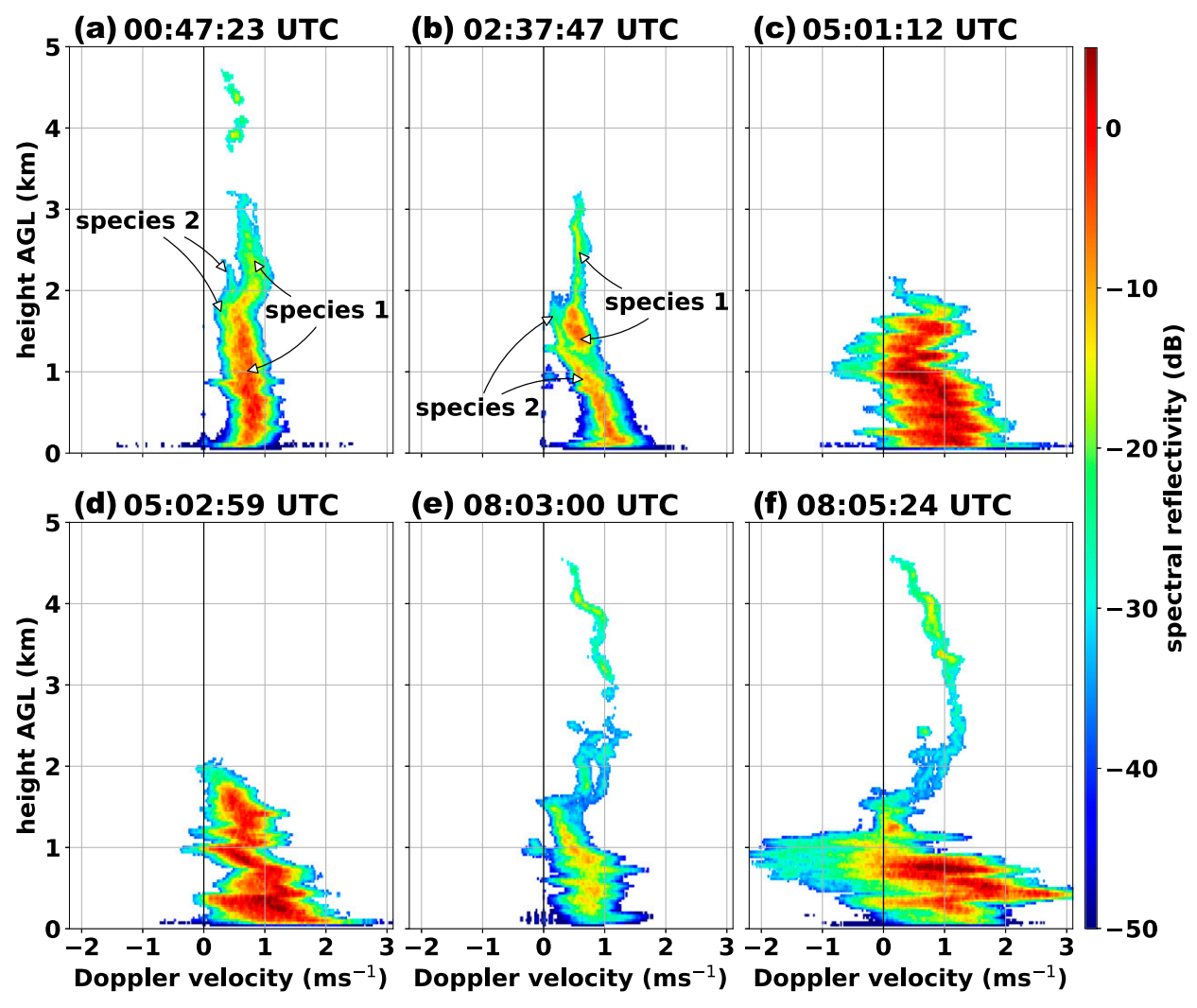


FIG. 7. Example KAZR Doppler spectrum measurements on 21 Oct 2016 at times indicated by the vertical dashed lines in Fig. 6.

dominant only at altitudes higher than about 1.4–1.5 km. In contrast to the 0047 UTC time moment, the spectra of the two species apparently do not merge but rather species 2 grows at the expense of species 1. This is consistent with hydrometeor aspect ratio retrievals for the corresponding time period (Fig. 3b), which indicate hydrometeors with aspect ratios of ~0.6–0.9 above these altitudes, and very nonspherical particles below about 1.4 km. Ground-based MASC images during this time interval (Fig. 5, row b) also confirm the dominance of species 2, showing only limited particle riming corresponding to the modest amounts of supercooled liquid. The signal from cloud liquid can be seen in the spectrum at a height of about 1 km at small absolute values of vertical Doppler velocity.

The Doppler spectrum measurements during the 0500–0506 UTC time interval (Figs. 7c,d) approximately correspond to the heaviest snowfall observed during the 21 October 2016 event. A presence of significant turbulence is evident throughout the whole hydrometeor layer. During this time

period there are no obvious spectral features that could help to differentiate among hydrometeor species with different fall velocities even though the MASC imaginary (Fig. 5, row c) indicates a mix of various particle types. Aspect ratio retrievals (Fig. 3c), however, suggest that aloft, along some of SACR2 slant beam azimuthal directions (e.g., 270° or 315°), single unrimed dendrites/plates can dominate radar backscatter. Aspect ratios of  $\sim\!0.4\!\!-\!\!0.5$  near the surface represent the mean values for the different hydrometer types observed by the MASC.

Some of the largest values of supercooled LWP were observed at the end of the SACR2 RHI scan period of 0800–0806 UTC (Fig. 2c). Such conditions favor production of graupel, which was observed at the ground. The Doppler measurements during this time (Fig. 7f) show substantial downward vertical Doppler velocities, likely indicating a significant amount of riming (e.g., Mosimann 1995) and a turbulent atmosphere. At earlier times during this interval reflectivities and mean velocities were smaller (Fig. 7e). As for

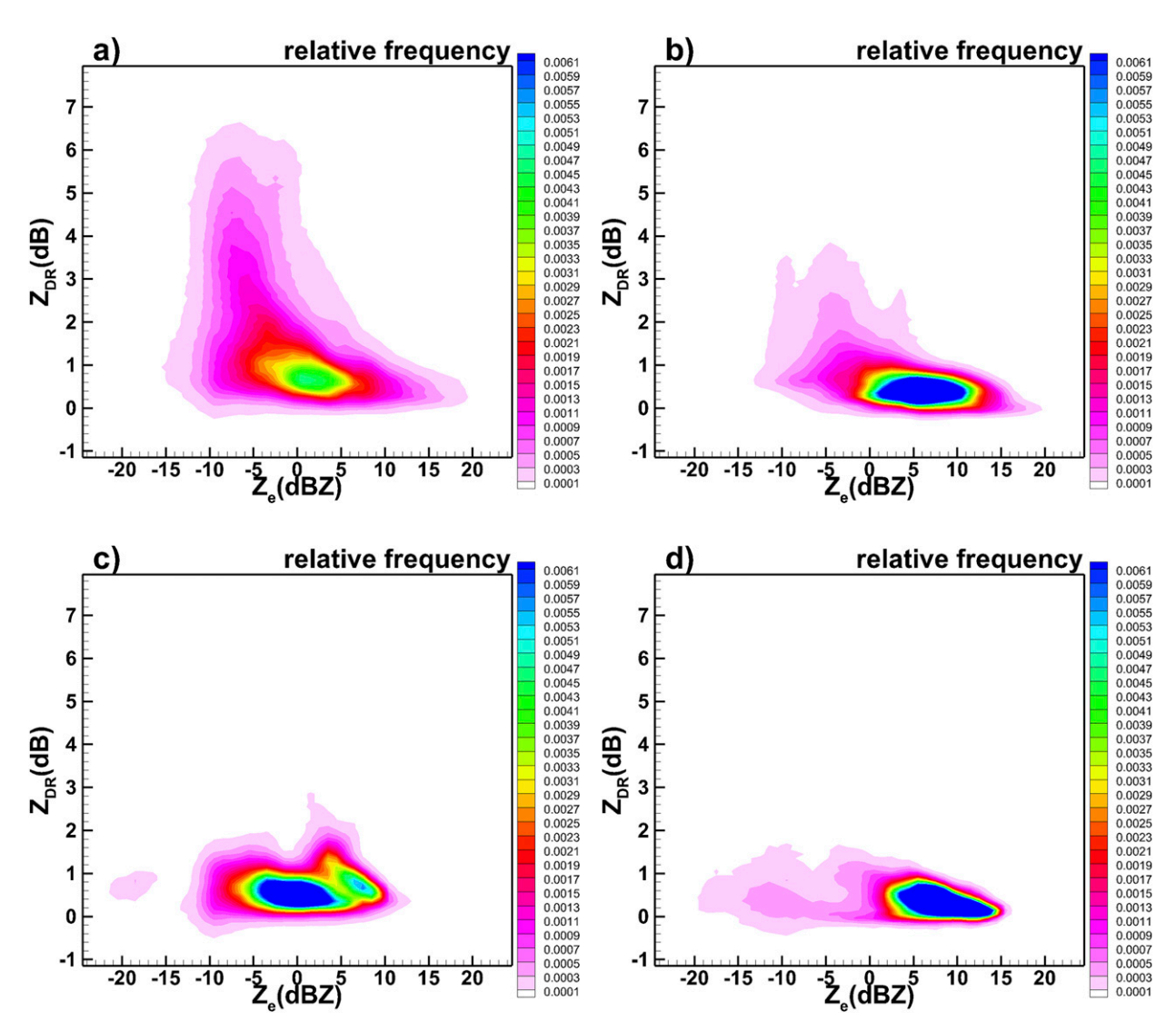


FIG. 8. Frequency scatterplot of reflectivity vs differential reflectivity SACR2  $K_a$ -band measurements in snowfall observed on (a) 21 Oct 2016, (b) 8 Nov 2016, (c) 9 May 2017, and (d) 14 May 2017; the  $Z_e$  and  $Z_{DR}$  bin sizes are 1 and 0.1 dB, respectively. Sample sizes for different events varied from  $\sim 2.5 \times 10^6$  to  $\sim 1.1 \times 10^7$ .

the 0500–0506 UTC RHI scan interval, identifying different particle types during the period of 0800–0806 UTC from Doppler spectrum measurements below 1.5 km is not obvious, even though retrievals indicate significant variability in hydrometeor aspect ratios observed at different 40° elevation SACR2 beam azimuth angles. MASC images also suggest that rimed single dendrites, which are more nonspherical compared to graupel particles, were also present in the hydrometeor mixture.

Note also that the Doppler measurements in all panels of Fig. 7 reveal spectral features near the height of 1 km either indicative of cloud water with Doppler velocity close to zero (clearly visible in Figs. 7a, 7b, and 7e) or significant updrafts manifested by negative downward velocities (in Figs. 7c and 7f). These updrafts are consistent with strong LWP enhancements indicating the presence of supercooled water that

accentuates a significant role of riming in snow formation during these periods.

## 3. Mean correspondence between reflectivity and differential reflectivity

Since differential reflectivity  $Z_{\rm DR}$  depends on hydrometeor shape and is directly measured by the SACR2, it is of particular interest to analyze if there is some mean correspondence between  $Z_{\rm DR}$  and  $Z_e$ , in snow, as previously observed in rain (e.g., Matrosov et al. 2016). Because  $Z_{\rm DR}$  is most pronounced for slant viewing and diminishes with increasing radar elevation, the low-elevation-angle PPI measurements are suitable for such an analysis.

For the snowfall event of 21 October 2016, Fig. 8a shows a  $Z_e$ – $Z_{\rm DR}$  frequency-of-occurrence scatterplot from SACR2 measurements at a 5° PPI scan with SNR exceeding 5 dB and

including measurement ranges less than 12 km. At these ranges and elevation angles, this scatterplot is indicative of the variability of radar parameters in clouds and precipitation occurring below about 1-km altitude. Lower-elevation-angle measurements (i.e.,  $3^{\circ}$ ) were not used because of strong ground clutter from industrial facilities at Oliktok Point. Modest ground clutter and beam blockage at some azimuth directions exists even in the  $5^{\circ}$  PPI scans (Matrosov 2020). The radar measurements from areas impacted by this clutter/blockage were excluded from further analysis. To alleviate possible influences of  $Z_{\rm DR}$  biases, SACR2 differential reflectivity data were calibrated in a relative sense using vertical radar beam measurements.

Unlike polarimetric radar variables, reflectivity needs to be calibrated in the absolute sense. Accurate absolute radar calibration is difficult to achieve (e.g., Maahn et al. 2019). Comparisons of closely collocated measurements by the SACR and the KAZR, when the former is pointing vertically, indicated a relative difference of about 2 dB (not shown). It was further assumed that this value is characteristic of the uncertainties of reflectivity measurements shown in Fig. 8.

Figure 8a shows  $Z_e$ – $Z_{\rm DR}$  correspondence for the 21 October 2016 event and indicates that, at low reflectivities ( $Z_e$  < 0 dBZ),  $Z_{\rm DR}$  values cover a large interval ranging from more than 6 to around 0 dB, which can be attributed to quasispherical hydrometeor shapes. Higher  $Z_{\rm DR}$  (e.g., > 6 dB) is characteristic of the branched planer crystals such as single pristine dendrites (e.g., Schrom and Kumjian 2018) and hexagonal plates (e.g., Matrosov 1991), which were observed in the lower atmospheric layers during this event (Fig. 3a).

Hydrometeor populations with larger reflectivities tend to exhibit smaller  $Z_{\rm DR}$  values. For very strong reflectivities (e.g.,  $Z_e > 20~{\rm dB}Z$ ), differential reflectivities are generally only a few tenths of 1 dB. Some general tendency of  $Z_{\rm DR}$  to decrease with increasing  $Z_e$  is present. This tendency is also, in part, due to decreasing bulk density of hydrometeor populations as particle characteristic sizes (and corresponding reflectivities) increase and mean particle shapes change.

To illustrate the event-to-event variability in the correspondence between reflectivity and differential reflectivity in snowfall, Figs. 8b–d show  $Z_e$ – $Z_{\rm DR}$  scatterplots for three other representative snowfall events observed at Oliktok Point on 8 November 2016, 9 May 2017, and 14 May 2017.  $Z_{\rm DR}$  data from PPI measurements during these events were generally smaller than those from the 21 October 2016 snowfall. Lower  $Z_{\rm DR}$  values for these other events suggest that single pristine crystals generally were not the dominant hydrometeor habits (at least not at lower altitudes covered by the PPI scans) during these other events. However,  $Z_e$ – $Z_{\rm DR}$  correspondences for higher reflectivities, when  $Z_{\rm DR}$  values are generally lower than those observed in areas with weaker reflectivities, are rather similar across different snowfall events.

## 4. Variability of particle shapes with temperature and reflectivity

Analyzing variability of particle shapes with temperature is of particular interest to this study. Frequency scatterplots of retrieved hydrometer aspect ratios versus ambient air temperature are depicted in Fig. 9. The temperature and aspect ratio bin sizes are 3°C and 0.1, and the total sample sizes are 4441, 6703, 5709, and 2046 in Figs. 9a-d, respectively. Note that each sample represents an aspect ratio retrieval averaged for  $40^{\circ} \pm 3^{\circ}$  beam elevations and five 0.03-km radar range gate intervals. As seen from comparing the panels of Fig. 9, retrieved aspect ratios of less than about 0.3 generally exist at temperatures warmer than about -17°C for all the events. At colder temperatures, particle aspect ratios usually vary approximately between 0.3 and 0.8, with most frequent values of  $\sim 0.5$ . Near the ground in a temperature range between approximately -7° and -4°C, these ratios vary in a larger range (most frequently between 0.2 and 0.8) with a mean value of  $\sim 0.5$ . There are, however, occurrences of very low aspect ratio hydrometeors there, indicating that some pristine crystals reach the lowest heights without being significantly affected by riming and/or aggregation processes that cause particles to become more spherical. The existence of very nonspherical particles is seen (Fig. 9a) at times when single pristine dendrites/plates were the dominant hydrometeor habits at the lower altitudes (e.g., Fig. 3b).

A change in ice hydrometeor mean aspect ratios at ambient air temperatures approximately from  $-15^{\circ}$  to  $-17^{\circ}$ C is most likely due to the presence of single planar crystals in the hydrometeor mixtures. The lowest particle aspect ratio values are retrieved when such crystals dominate radar returns. Regions where very nonspherical particles contribute significantly to radar returns aloft exist for all the events shown though magnitudes of these contributions vary. Such particles, however, do not necessarily carry through to the lowest layers, as they do during periods of the 21 October 2016 event. It can also be seen from the low-elevation-angle PPI differential reflectivity data (e.g., Figs. 8c,d, where high  $Z_{\rm DR}$  values are absent).

While the evidence supporting the presence of low-aspectratio hydrometeors during times with temperatures warmer than approximately from  $-17^{\circ}$  to  $-15^{\circ}\mathrm{C}$  is a common feature in Fig. 9, sometimes the increased occurrence is seen starting at somewhat warmer temperatures (e.g., Fig. 9b). It could be, in part, due to uncertainties of interpolating ambient air temperature from only two daily radiosonde soundings. Hydrometeors with very low aspect ratios at air temperatures warmer than approximately from  $-17^{\circ}$  to  $-15^{\circ}\mathrm{C}$  are observed during the 21 October 2016 event more often than for other events shown in Fig. 9. A general decrease in the frequency of occurrence of very nonspherical particles with small aspect ratios at warmer temperatures (e.g.,  $\sim -7^{\circ}\mathrm{C}$ ) is likely due to aggregation and/or riming processes.

Figure 10 shows scatterplots of retrieved particle aspect ratios versus reflectivity measurements. Trends indicating hydrometeor aspect ratio decreases with increasing reflectivities could be seen for reflectivities less than about  $-10\,\mathrm{dB}Z$ . The occurrence of hydrometeors with aspect ratios less than about 0.2 is most often seen when reflectivities are approximately between -10 and  $10\,\mathrm{dB}Z$ . They are likely associated with pristine and lightly rimed planar-type crystals. This finding is consistent with data shown in Fig. 8, where the largest  $Z_{\mathrm{DR}}$  values are observed for a similar reflectivity range.

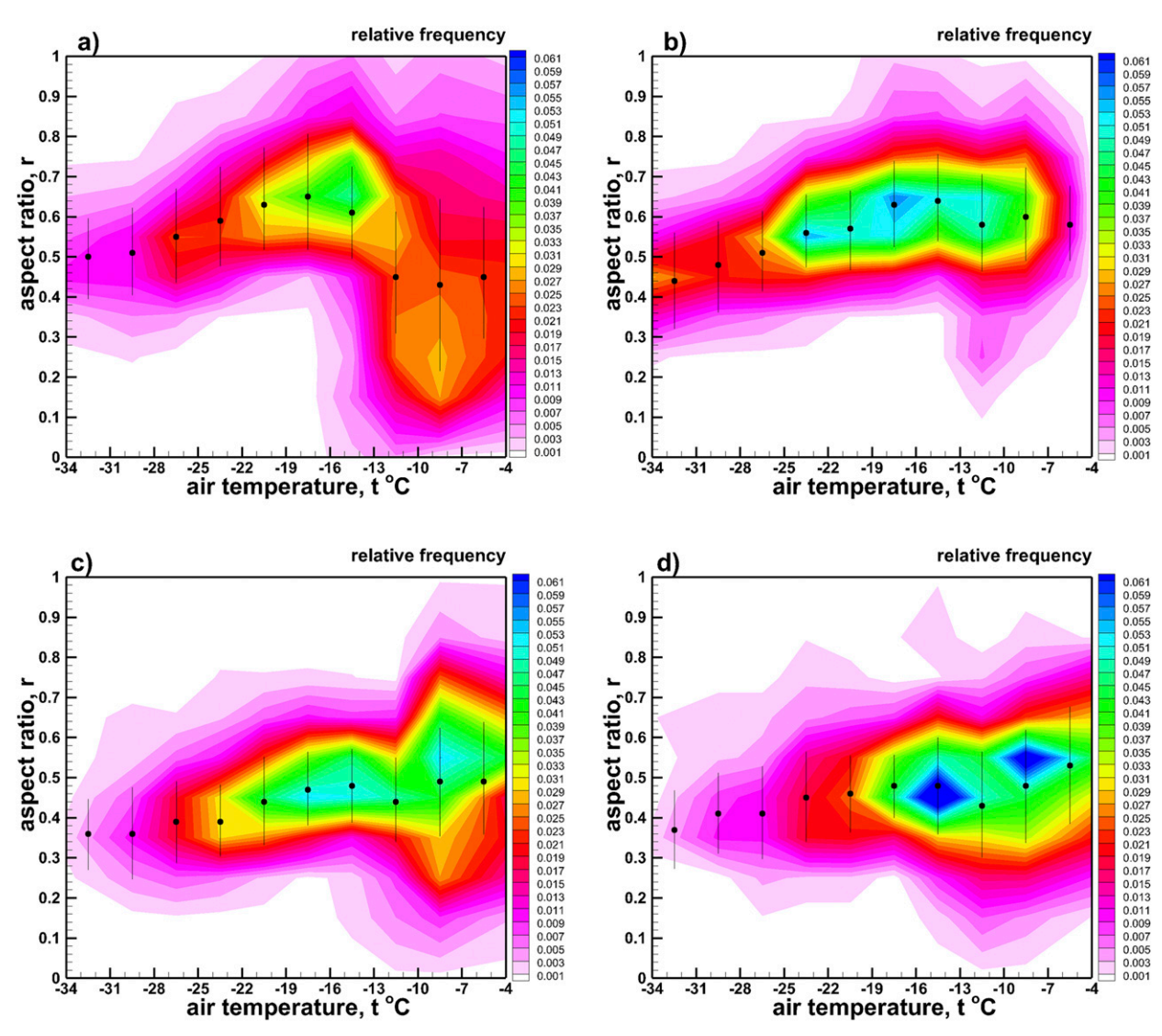


FIG. 9. As in Fig. 8, but for retrieved ice hydrometeor aspect ratios vs temperature. Symbols show mean aspect ratios in 3°C temperature bins. Thin vertical lines indicate mean values (dots) ± standard deviations.

An increase in the frequency of occurrence and a secondary weak frequency maximum corresponding to crystals with aspect ratios less than 0.2 at  $Z_e \approx -2\,\mathrm{dB}Z$  is seen for the event of 21 October 2016 (Fig. 10a). However, such increases are less pronounced in the other panels of Fig. 10. These increases generally occur when  $Z_e$  is approximately between -5 and  $5\,\mathrm{dB}Z$ . Larger-size hydrometeor populations resulting in higher reflectivity values are dominated by more spherical particles (e.g., aggregates) and could mask smaller crystals with lower aspect ratios even if such crystals are present in a mixture.

#### 5. Discussion and conclusions

The main objective of this study was to evaluate the variability of ice hydrometeor aspect ratios in snowfall based on polarimetric radar-based retrievals. A remote sensing method

to retrieve average shapes of ice hydrometeors, as defined by their aspect ratios (i.e., particle minor-to-major dimension ratios), was applied to K<sub>a</sub>-band scanning polarimetric radar measurements at the DOE ARM mobile facility deployed at Oliktok Point, Alaska. This method is based on the use of circular depolarization ratios,  $CDR_p$ , which are reconstructed from direct radar measurements of differential reflectivity,  $Z_{\rm DR}$ , and the copolar correlation coefficient,  $\rho_{hv}$ , measured by the scanning SACR2 system. Compared to traditional polarimetric radar variables in the horizontal-vertical polarization basis, CDR<sub>p</sub>-based estimates are less susceptible to hydrometeor orientation and thus more suitable for particle shape retrievals. Reflectivity measurements were also used to estimate characteristic sizes of hydrometeor populations, which allows for approximate accounting of bulk density changes with particle size.

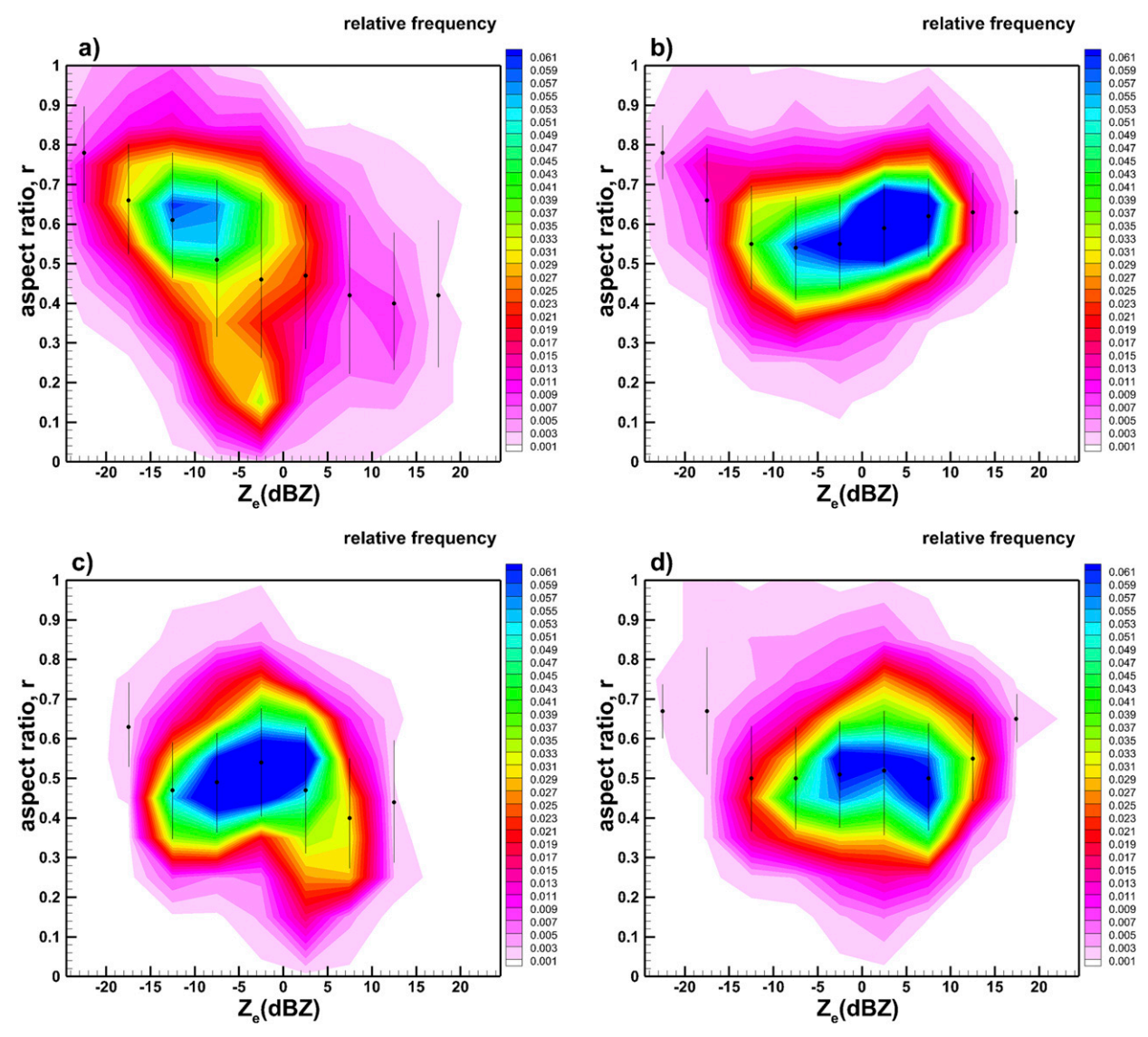


FIG. 10. As in Fig. 9, but for retrieved ice hydrometeor aspect ratios vs K<sub>a</sub>-band reflectivity. Reflectivity bins are 5 dB wide.

Overall retrievals were performed for four snowfall events. SACR2 RHI measurement sequences were used for retrievals. Retrieved vertical profiles of hydrometeor aspect ratios and measurements from radiosonde soundings were used to analyze temperature dependencies of particle shapes. The retrievals indicated that at ambient air temperatures colder than approximately -20°C, aspect ratios of ice hydrometeors generally vary approximately between 0.3 and 0.8. Lower values of particle aspect ratios are often retrieved at warmer ambient air temperatures starting approximately from  $-17^{\circ}$  to  $-15^{\circ}$ C. This can be explained by the growth of pristine planar crystals of dendritic and hexagonal plate habits in the temperature regime around  $-15^{\circ}$ C. At warmer temperatures, the variability of hydrometeor aspect ratios is usually large (Fig. 9) as particle habits could vary from pristine crystals, which can reach lower

heights without being significantly affected by riming and/or aggregation, to significantly aggregated or/and heavily rimed hydrometeors, which have larger aspect ratios. The lowest hydrometeor aspect ratio values were most often observed when reflectivities were approximately between  $-10 \ {\rm and} \ 10 \ {\rm dB}Z$  (Fig. 10). Observations with high reflectivities are usually dominated by larger aggregated and/or rimed particle populations, which also tend to be more spherical.

Although the increased occurrence of hydrometeors with lower aspect ratios (e.g., r < 0.3) for temperatures warmer than approximately from  $-17^{\circ}$  to  $-15^{\circ}$ C was observed for all snowfall events, it was seen the most profoundly in the 21 October 2016 data (Fig. 9a). Some of the smallest aspect ratio values were retrieved during this event. This is because this event had periods when single pristine dendrites and

hexagonal plates were the dominant habits in the layer below approximately  $1.6\text{-}2\,\mathrm{km}$  and were falling to the ground without being significantly affected by aggregation and riming (e.g., Fig. 3b). Given the occurrence of such crystals as dominant species at lower heights, this event was also characterized by the periods of very high differential reflectivity values ( $\sim 6\,\mathrm{dB}$ ) observed during the low radar elevation SACR2 PPI measurements (e.g., Fig. 8a). While the occurrence of single pristine crystals as a dominant species (especially near the ground) is not a very common situation, is not unique either (e.g., Matrosov et al. 2019). More often, however, more spherical aggregated and/or rimed hydrometeors dominate radar echoes at lower altitudes with warmer temperatures. As a result, low-elevation-angle  $Z_{\mathrm{DR}}$  values are relatively small (e.g., Figs. 8c,d).

Results of the polarimetric radar-based hydrometeor aspect ratio retrievals were generally consistent with visual information provided by hydrometeor images from the MASC. These images allowed for qualitative estimation of the dominant particle habits during different RHI radar scanning intervals when aspect ratio retrievals were performed. The lowest retrieved aspect ratios (e.g., < 0.3) near the ground were obtained when the MASC indicated pristine and lightly rimed single planar crystals as a dominant hydrometeor type. Larger aspect ratios of around 0.6 or so were retrieved near the ground when relatively "blocky" aggregates and/or air regular shape particles were observed by the MASC. Periods of increased supercooled liquid water path, as inferred from the collocated microwave radiometer measurements, usually corresponded to a mixture of different particle habits as photographed by the MASC and intermediate values of retrieved aspect ratios (e.g., ~0.4-0.5). Periods of higher LWP values also often corresponded to increased snowfall rates and significantly rimed particles were observed during such periods.

Doppler spectra from the vertically pointing KAZR provide some additional information on the existence of different hydrometeors species as a function of height. This additional information is most helpful for situations when particle habits are more uniform horizontally, which ensures that SACR2 based aspect ratio retrievals do not vary very significantly depending on the azimuthal direction of the radar beam (e.g., periods shown in Figs. 3a and 3b corresponding respectively to Figs. 7a and 7b). The Doppler spectrum data can potentially be used for estimating relative contributions of different species to radar variables if such species are identifiable by the separate spectral peaks. While vertical Doppler measurements are not directly informative of hydrometeor shapes, they (when multiple particle populations are present) can be used to identify the dominant hydrometeor species influencing hydrometeor shape retrievals from scanning polarimetric radar measurements.

Low-elevation-angle SACR2 measurements of snowfall indicate, on average, a decreasing differential reflectivity,  $Z_{\rm DR}$ , trend when reflectivity,  $Z_e$ , increases. The largest values of  $Z_{\rm DR}$  and its greatest variability are often observed when  $Z_e$  is between -10 and 0 dBZ. Relative to other snowfall events, the frequency of occurrence of the largest  $Z_{\rm DR}$  values during the 21 October 2016 event was enhanced as a result of periods

during which single dendrites/plates with low aspect ratios were the dominant hydrometeor habits. At larger reflectivities, variability in  $Z_{\rm DR}$  decreases as particles generally become more spherical due to riming and aggregation and their size increases. Aggregation also reduces particle bulk density.

Measurements and retrievals such as those presented in the current study offer insight into microphysical processes in ice-containing clouds, including climatologically important Arctic mixed-phase clouds. This information can be used to evaluate and improve numerical prediction tools to support weather and climate forecasting and bolster fundamental understanding of atmospheric physics. An extension of the current study could involve the application of the remote sensing method used here for retrievals across a wider range of precipitation events including those observed by comparable sensors in other geographical regions.

Acknowledgments. The research outlined in this paper was supported by the U.S. Department of Energy (DOE) Atmospheric Systems Research (ASR) program under project DE-SC0013306 and the National Science Foundation (Grant AGS 1841260). The field operators of the DOE Atmospheric Radiation Measurement (ARM) third mobile facility (AMF3) are recognized for their dedication and hard work to keep the instruments collecting the data analyzed here up and running through harsh weather conditions.

#### REFERENCES

Bailey, M. P., and J. Hallett, 2009: A comprehensive habit diagram for atmospheric ice crystals: Confirmation from the laboratory, AIRS II, and other field studies. J. Atmos. Sci., 66, 2888– 2899, https://doi.org/10.1175/2009JAS2883.1.

Bukovčić, P., A. Ryzhkov, D. Zrnić, and G. Zhang, 2018: Polarimetric radar relations for quantification of snow based on disdrometer data. J. Appl. Meteor. Climatol., 57, 103–120, https://doi.org/10.1175/JAMC-D-17-0090.1.

Fukuta, N., and T. Takahashi, 1999: The growth of atmospheric ice crystals: A summary of findings in vertical supercooled cloud tunnel studies. J. Atmos. Sci., 56, 1963–1979, https://doi.org/ 10.1175/1520-0469(1999)056<1963:TGOAIC>2.0.CO;2.

Garrett, T. J., S. E. Yuter, C. Fallgatter, K. Shkurko, S. R. Rhodes, and J. L. Endries, 2015: Orientations and aspect ratios of falling snow. *Geophys. Res. Lett.*, 42, 4617–4622, https://doi.org/10.1002/ 2015GL064040.

Giangrande, S., and T. Toto, 2013: Interpolated sonde (INTERPOLATEDSONDE); ARM Mobile Facility (OLI) Oliktok Point, Alaska; AMF3 (M1) (updated hourly). ARM Climate Research Facility Data Archive, accessed 19 April 2017, https://doi.org/10.5439/1095316.

Griffin, E., T. Schuur, and A. Ryzhkov, 2018: A polarimetric analysis of ice microphysical processes in snow, using quasivertical profiles. *J. Appl. Meteor. Climatol.*, 57, 31–50, https:// doi.org/10.1175/JAMC-D-17-0033.1.

Hardin, J., D. Nelson, I. Lindenmaier, B. Isom, K. Johnson, A. Matthews, and N. Bharadwaj, 2011: ARM: Ka-band scanning ARM cloud radar hemispherical sky RHI scan (KASACRHSRH). Subset used: 708N29042.8900N, 149853012.7800W: Oliktok Point Mobile Facility (M1), ARM Climate Research Facility Data Archive, accessed 8 October 2017, https://doi.org/10.5439/1046197.

- Hashino, T., and G. J. Tripoli, 2008: The Spectral Ice Habit Prediction System (SHIPS). Part II: Simulation of nucleation and depositional growth of polycrystals. *J. Atmos. Sci.*, 65, 3071–3094, https://doi.org/10.1175/2008JAS2615.1.
- Heymsfield, A. J., Z. Wang, and S. Y. Matrosov, 2005: Improved radar ice water content retrieval algorithms using coincident microphysical and radar measurements. *J. Appl. Meteor.*, **44**, 1391–1412, https://doi.org/10.1175/JAM2282.1.
- Isom, B., N. Bharadwaj, I. Lindenmaier, D. Nelson, J. Hardin, and A. Matthews, Eds., 2018: Ka-band scanning ARM cloud radar (KASACRPPIVH); ARM Mobile Facility (OLI) Oliktok Point, Alaska, AMF3 (M1). ARM Data Center, accessed 9 January 2020, https://doi.org/10.5439/1224837.
- Jensen, A. A., J. Y. Harrington, H. Morrison, and J. A. Milbrandt, 2017: Predicting ice shape evolution in a bulk microphysics model. J. Atmos. Sci., 74, 2081–2104, https://doi.org/10.1175/ JAS-D-16-0350.1.
- Kollias, P., and Coauthors, 2020: The ARM radar network: At the leading-edge of cloud and precipitation observations. *Bull. Amer. Meteor. Soc.*, **101**, E588–E607, https://doi.org/10.1175/BAMS-D-18-0288.1.
- Korolev, A., and G. Isaac, 2003: Roundness and aspect ratio of particles in ice clouds. *J. Atmos. Sci.*, **60**, 1795–1808, https://doi.org/10.1175/1520-0469(2003)060<1795:RAAROP>2.0.CO;2.
- Maahn, M., 2019: MASC snow particle images; ARM Mobile Facility (OLI) Oliktok Point, Alaska; AMF3 (M1). ARM Data Center, accessed 21 February 2019, https://doi.org/ 10.5439/1497701.
- —, F. Hoffmann, M. D. Shupe, G. de Boer, S. Y. Matrosov, and E. P. Luke, 2019: Can liquid cloud microphysical processes be used for vertically pointing cloud radar calibration? *Atmos. Meas. Tech.*, 12, 3151–3171, https://doi.org/10.5194/amt-12-3151-2019.
- Magono, C., and C. W. Lee, 1966: Meteorological classification of natural snow crystals. J. Fac. Sci. Hokkaido Univ., Ser. 7, 2, 321–335.
- Matrosov, S. Y., 1991: Theoretical study of radar polarization parameters obtained from cirrus clouds. *J. Atmos. Sci.*, **48**, 1062–1070, https://doi.org/10.1175/1520-0469(1991)048<1062: TSORPP>2.0.CO;2.
- —, 1997: Variability of microphysical parameters in high-altitude ice clouds: Results of the remote sensing method. *J. Appl. Meteor.*, **36**, 633–648, https://doi.org/10.1175/1520-0450-36.6.633.
- —, 2020: Ice hydrometeor shape estimations using polarimetric operational and research radar measurements. *Atmosphere*, 11, 97, https://doi.org/10.3390/atmos11010097.
- —, and A. J. Heymsfield, 2017: Empirical relations between size parameters of ice hydrometeor populations and radar reflectivity. J. Appl. Meteor. Climatol., 56, 2479–2488, https:// doi.org/10.1175/JAMC-D-17-0076.1.
- —, and D. D. Turner, 2018: Retrieving mean temperature of atmospheric liquid water layers using microwave radiometer measurements. *J. Atmos. Oceanic Technol.*, 35, 1091–1102, https://doi.org/10.1175/JTECH-D-17-0179.1.
- —, R. F. Reinking, R. A. Kropfli, B. E. Martner, and B. W. Bartram, 2001: On the use of radar depolarization ratios for estimating shapes of ice hydrometeors in winter clouds. J. Appl. Meteor., 40, 479–490, https://doi.org/10.1175/1520-0450(2001)040<0479:OTUORD>2.0.CO;2.
- ——, M. D. Shupe, and I. V. Djalalova, 2008: Snowfall retrievals using millimeter-wavelength cloud radars. J. Appl. Meteor. Climatol., 47, 769–777, https://doi.org/10.1175/2007JAMC1768.1.

- —, G. G. Mace, R. Marchand, M. D. Shupe, A. G. Hallar, and I. B. McCubbin, 2012: Observations of Ice crystal habits with a scanning polarimetric W-band radar at slant linear depolarization ratio mode. *J. Atmos. Oceanic Technol.*, 29, 989–1008, https://doi.org/10.1175/JTECH-D-11-00131.1.
- —, R. Cifelli, P. J. Neiman, and A. B. White, 2016: Radar rainrate estimators and their variability due to rainfall type: An assessment based on Hydrometeorology Testbed data from the southeastern United States. *J. Appl. Meteor. Climatol.*, 55, 1345–1358, https://doi.org/10.1175/JAMC-D-15-0284.1.
- —, C. G. Schmitt, M. Maahn, and G. de Boer, 2017: Atmospheric ice particle shape estimates from polarimetric radar measurements and in situ observations. *J. Atmos. Oceanic Technol.*, 34, 2569–2587, https://doi.org/10.1175/JTECH-D-17-0111.1.
- —, M. Maahn, and G. de Boer, 2019: Observational and modeling study of ice hydrometeor radar dual-wavelength ratios. J. Appl. Meteor. Climatol., 58, 2005–2017, https://doi.org/10.1175/JAMC-D-19-0018.1.
- Matthews, B., B. Isom, D. Nelson, I. Lindenmaier, J. Hardin, K. Johnson, and N. N Bharadwaj, 2015: Ka ARM zenith radar (KAZRGE); ARM Mobile Facility (OLI) Oliktok Point, Alaska; AMF3 (M1) (updated hourly). ARM Climate Research Facility Data Archive, accessed 9 January 2020, https://doi.org/ 10.5439/1025214.
- Melnikov, V., 2017: Parameters of cloud ice particles retrieved from radar data. *J. Atmos. Oceanic Technol.*, **34**, 717–728, https://doi.org/10.1175/JTECH-D-16-0123.1.
- Mosimann, L., 1995: An improved method for determining the degree of snow crystal riming by vertical Doppler radar. *Atmos. Res.*, 37, 305–323, https://doi.org/10.1016/0169-8095(94)00050-N.
- Myagkov, A., P. Seifert, M. Bauer-Pfundstein, and U. Wandinger, 2016: Cloud radar with hybrid mode towards estimation of shape and orientation of ice crystals. *Atmos. Meas. Tech.*, 9, 469–489, https://doi.org/10.5194/amt-9-469-2016.
- Oue, M., P. Kollias, A. Ryzhkov, and E. Luke, 2018: Towards exploring the synergy between cloud radar polarimetry and Doppler spectral analysis in deep cold precipitating systems in the Arctic. *J. Geophys. Res. Atmos.*, **123**, 2797–2815, https://doi.org/10.1002/2017JD027717.
- Pruppacher, H. R., and J. D. Klett, 1978: *Microphysics of Clouds and Precipitation*. D. Reidel, 714 pp.
- Reinking, R. F., S. Y. Matrosov, R. A. Kropfli, and B. W. Bartram, 2002: Evaluation of a 45° slant quasi-linear radar polarization for distinguishing drizzle droplets, pristine ice crystals, and less regular ice particles. *J. Atmos. Oceanic Technol.*, **19**, 296–321, https://doi.org/10.1175/1520-0426-19.3.296.
- Ryzhkov, A. V., and D. S. Zrnić, 2019: Radar Polarimetry for Weather Observations. Springer, 486 pp.
- —, and Coauthors, 2017: Estimation of depolarization ratio using weather radars with simultaneous transmission/reception. J. Appl. Meteor. Climatol., 56, 1797–1816, https://doi.org/ 10.1175/JAMC-D-16-0098.1.
- Schrom, R. S., and M. R. Kumjian, 2018: Bulk-density representations of branched planar ice crystals: Errors in the polarimetric radar variables. *J. Appl. Meteor. Climatol.*, 57, 333–346, https://doi.org/10.1175/JAMC-D-17-0114.1.
- Vogel, J. M., and F. Fabry, 2018: Contrasting polarimetric observations of stratiform riming and nonriming events. *J. Appl. Meteor. Climatol.*, 57, 457–476, https://doi.org/10.1175/JAMC-D-16-0370.1.